Reactive transport and sorption behavior of pollutants in presence of redox-sensitive nano Fe^0 impregnated graphene: Advancing towards continuous water filtration

Jai Kishan Rajak [a,b], Nitin Khandelwal [c,*], Zahid Ahmad Ganie [a], Dieter Schild [d], Gopala Krishna Darbha [a,e]

[a] Environmental Nanoscience Laboratory, Department of Earth Sciences, IISER Kolkata, Mohanpur 741246 West Bengal,India
[b] Particle Engineering Centre, Department of Chemical Engineering, Norwegian University of Science and Technology, Trondheim 7941, Norway
[c] Department of Hydrology, Indian Institute of Technology (IIT) Roorkee, Roorkee 247667 Uttarakhand, India
[d] Karlsruhe Institute of Technology (KIT), Institute for Nuclear Waste Disposal, Hermann-von-Helmholtz-Platz 1, 76344 Eggenstein-Leopoldshafen, Germany
[e] Center for Climate & Environmental Studies, IISER Kolkata, Mohanpur 741246 West Bengal, India

Keywords:
Graphene
Water purification
Metals sorption
Dyes removal
Reduction
Column treatment

A B S T R A C T

Fe^0 impregnated graphene has shown promising candidature for removing both organic and inorganic contaminants from aqueous solutions. The current study investigates and fills some of the missing gaps in their large-scale environmental applicability, including- contaminants removal from complex water matrices, simultaneous separation of multiple contaminants, and continuous water filtration possibilities. Both metals and dyes were chosen of varying ionic behavior to broaden the scope of the work.

One-step graphene oxide (GO) delamination and iron reduction were performed to prepare Fe^0 impregnated graphene (GOI) composite. Results have shown growth of smaller spherical Fe^0 nanoparticles (< 50 nm) on graphene with good dispersion and preserved redox state. XPS analysis of reaction precipitate confirmed that GOI could reduce CrO_4^{2-} to less toxic Cr(III) through reductive sorption. Removal capacities in batch mode were Ni (30.5 mg/g) < Cr (49.8 mg/g) < Cd (93.7 mg/g) < As (143.6 mg/g) in mono-metallic system. In a multi-metallic system, efficient total metal removal capacity (>340 mg/g) and continuous filtration efficiency (85 mg/g) was observed. GOI composite has also shown efficient removal and continuous separation of cationic methylene blue (81.3 mg/g), anionic methyl orange (79.7 mg/g), and zwitterionic rhodamine-B (31.7 mg/g). Electrostatic attraction on heterogeneous GOI surface, redox transformation, complexation, and co-precipitation with generated iron-oxy-hydroxide were major contaminant removal mechanisms. Results conclude a good potential of GOI composite in the separation of multiple pollutants from environmental matrices and continuous filtration of contaminated waters.

1. Introduction

The tremendous increase in world population intensified agricultural and industrial activities resulting in the release of hazardous pollutants in water bodies. Freshwater scarcity and unavailability of safe drinkable water are causing ecosystem imbalance and posing severe impacts on human health. Simultaneous contamination of water bodies with multiple pollutants is a major challenge among the scientific community, which requires immediate attention and innovative solutions.

Nanotechnology has bloomed in several sectors, and in the last two decades, researchers have vastly explored the potential of nanomaterials in environmental applications. Their unique properties, i.e., nanoscale size range, high specific surface area and surface tunability, make them highly reactive adsorbents to capture a wide range of pollutants (Das et al., 2017). In the series of emerging nanomaterials for environmental applications, graphene has apprehended the scientific community's attention (Perreault et al., 2015). Graphene is a 2D carbon sheet with all the atoms exposed on the surface in case of most ideal one atom thick layers, resulting in the highest surface material. (Sur, 2012; Dideikin and Vul, 2019) Due to its chemical stability, optical transparency, mechanical strength, electron mobility, and very high specific surface area; the application of graphene widened from electric industries to biomedical

* Corresponding author.
E-mail addresses: nitin.khandelwal@hy.iitr.ac.in (N. Khandelwal), gkdarbha@gmail.com (G.K. Darbha).

devices and environmental pollution remediator cum sensors (Perreault et al., 2015; Shen et al., 2015).

Graphene oxide (GO) and graphene-based nanomaterials have been explored as adsorbents, photocatalysts, contaminant monitoring electrodes or building blocks for filtration membranes (Plastiras et al., 2021; Nadres et al., 2016; Fanourakis et al., 2020). Graphene surfaces can provide efficient support to anchor various functionalities or to grow nanoparticles (Badhulika et al., 2015). In addition, various functional groups on GO sheets, i.e., OH, –COOH, C-O, etc., are hydrophilic in nature, resulting in suspension stability in aqueous media and providing nucleation sites for nanoparticles leading to well-dispersed particles on GO surface (Kruk and Warszyński, 2021). Therefore, graphene-based nanocomposites are at the forefront of environmental materials (Gupta et al., 2024). Redox-sensitive nanoparticles (RSNPs) such as Fe^0 can have electron transfer on the surface, which can result in reductive sorption of contaminants or organic degradation due to generated free radicals (Raman and Kanmani, 2016; Khandelwal et al., 2021; Khandelwal et al., 2023).

But prevention of self-aggregation and preservation of redox-state of RSNPs is crucial to ensure their enhanced electron transferability and reactivity for pollutants (Guan et al., 2015). Growth of RSNPs such as Fe^0 can result in initial storage of Fe^0 released electrons in GO layers and their later mobilization either to iron nanoparticles again or to the pollutants (Xing et al., 2020; Aher et al., 2019). This GO mediated electron storage and release can result in a multifold increase in the reactivity of Fe^0. Therefore, researchers have so far explored the potential of graphene oxide- elemental iron nanocomposite (GOI) in reductive sorption and degradation of a wide range of pollutants, including radionuclides, toxic metals, dyes, antibiotics, and other organic pollutants (Wang et al., 2015; Ren et al., 2019; Fan et al., 2017; Masud et al., 2020; Zhu et al., 2015; Li et al., 2015).

For example, in 2012, Zhang et al. have shown the possibility of decolorization for methyl orange within 30 min of interaction time using Fe-graphene composite (Zhang et al., 2012). Further, Wang et al. have shown removal of orange IV azo dye with 3-D graphene-Fe composite and suggested the possibility of both adsorption and redox reaction in the system (Wang et al., 2015). Further research on dye removal with graphene iron showed Fenton degradation as a possible mechanism for cationic methylene blue (MB) degradation using nZVI assembled on Fe_3O_4-reduced graphene oxide (RGO) composite. 98 % of MB (50 mg/L) removal was achieved at pH = 3 with 0.8 M H_2O_2 and 0.1 g/L composite (Yang et al., 2015). The requirement of acidic pH of the solutions limits the applicability in natural water bodies. Removal of other dyes such as Rhodamine B (RB) and Acid Red 18 was also investigated with different graphene-based Fe^0 composites (Xu et al., 2018; Mehrabi et al., 2019). But all these studies were performed in batch mode, limiting the understanding of the possibilities of continuous column separation of dyes. Also, the impact of environmental parameters and removal in natural matrices is still not well explored and crucial to ascertain real environmental applications. Similarly, in the field of toxic metals removal, in 2013, Jabeen et al. first reported the possibility of Pb^{2+} ions removal. They confirmed reductive sorption as a possible removal mechanism for graphene-nZVI composite. Further, the removal of both metal oxyanions and cations has been explored with various graphene-iron composites (Kumarathilaka et al., 2016; Li et al., 2016; Cao et al., 2018; Das et al., 2020). Removal of some of the toxic metals and radionuclides has also been investigated from complex water matrices (Yao et al., 2019; Pan et al., 2024). For instance, Ren et al. fabricated PVDF-GO-nZVI membranes via electrospinning, achieving efficient removal of Cd(II) (100 %) and TCE (82 %) through gravity-driven filtration. The addition of GO improved membrane hydrophilicity, enhanced filtration flux, and enabled nZVI immobilization, preventing aggregation (Ren et al., 2019). Recently, Liu et al. explored the remediation of groundwater nitrate (NO_3-N) and hexavalent chromium (Cr(VI)) using reduced graphene oxide-supported nanoscale zero-valent iron (rGO/nZVI). They demonstrated the material's high adsorption capacities for NO_3-N (18.03 mg/g) and Cr(VI) (94.70 mg/g) and its ability to form a stable in-situ reactive zone for continuous removal over 96 h. The study revealed a synergistic removal mechanism and highlighted xanthan gum's role in enhancing rGO/nZVI stability for aquifer applications (Liu et al., 2022). Jha et al. developed a waste biomass derived graphene oxide-nano zerovalent iron (GO-nZVI) composite for antibiotic removal which achieved 91 % and 92 % degradation efficiencies for tetracycline and ciprofloxacin, respectively in water, with non-toxic degradation products confirmed via microbial assays (Jha et al., 2024). However, critical scientific gaps still exist if real environmental applicability is considered, which are listed below-.

(i) Continuous column separation of toxic metal species and dyes of varying ionic nature has not been explored.
(ii) Treatment possibilities of waters contaminated with multi-metallic species in both batch and column mode have not been investigated so far.
(iii) Detailed analysis of the impact of environmental parameters and removal of monometallic species, multi-metals, and dyes from various water matrices (river water, groundwater, and seawater) is missing in the literature.

All the highlighted gaps have prime value in ascertaining broad environmental applicability and are the focus of the current study.

Here, we have explored sorption behavior and reactive transport of dyes and metals of varying ionic nature in the presence of graphene oxide-elemental iron nanocomposite (GOI). Studied contaminants include- metal cations (Ni^{2+}, and Cd^{2+}), oxy-anions (AsO_2^-, and CrO_4^{2-}) and cationic methylene blue (MB), anionic methyl orange (MO), and zwitterionic rhodamine-B (RB) dyes. Experiments were also performed in multi-metals contaminated water solutions. Detailed mechanistic insights were obtained via thorough surface characterization of reaction precipitates using XPS, pXRD, DLS, FTIR, and HRTEM, in addition to non-linear kinetic, isotherm, and column transport modeling. The impact of solution pH and various natural water matrices, i.e., river water, groundwater, and seawater, on the sorption behavior of GOI nanocomposite was also evaluated to justify the environmental applicability of the composite.

2. Materials and methods

2.1. Materials and chemicals

All purchased chemicals and materials were at least of analytical grade. For synthesis- $FeCl_3{\cdot}6H_2O$, Ethanol, $NaBH_4$, H_2SO_4, H_2O_2, and $KMnO_4$ were purchased from Merck. Graphite powder was procured from Loba Chemie Pvt. Ltd. India. Studied contaminants, i.e., $K_2Cr_2O_7$, $NaAsO_2$, $Ni(NO_3)_2{\cdot}6H_2O$, $CdCl_2{\cdot}2H_2O$, methyl orange, and methylene blue, were obtained from Merck, whereas Rhodamine-B was supplied by Sigma Aldrich (US). Other chemicals involve $NaNO_3$, NaCl, $CaCl_2$, Na_2SO_4, HCl, NaOH, $NaHCO_3$, and H_3PO_4, which were supplied by Merck. All stock solutions were prepared with 18.2 MΩ Milli-Q water.

2.2. Synthesis of graphite oxide bulk

Modified Hummers method was used to prepare graphene oxide (Shukla et al., 2017). In brief, 1 g of graphite powder was mixed with 0.5 g $NaNO_3$ and added to 23 mL of H_2SO_4 in an ice water bath. In slow stirring mode, 3 g of $KMnO_4$ was added to the system, and shaking was continued for the next 2 h. After that, the cold mixture solution was transferred to a 35 °C water bath and further stirred for 30 min. Then 46 mL of water was added, and the temperature was maintained at 98 °C. To terminate the reaction, 10 mL of H_2O_2 and 140 mL of water were added to the system. The dark yellow-colored mixture was filtered and washed with 5 % HCl. Then the obtained graphite oxide powder was repeatedly washed with water and dried in a vacuum at 60 °C.

2.3. Synthesis of GO and GOI composite

Graphite oxide powder (1 g) was added to 4:1 ethanol–water solution and sonicated to 30 min for proper delamination of sheets and GO generation. After that, $FeCl_3{\cdot}6H_2O$ was added in 1:1 Fe-GO mass ratio to the suspension, and sonication continued further for 30 min as optimized in earlier publications for other iron composites (Khandelwal et al., 2023; Khandelwal et al., 2020). To assure homogeneous interaction and sorption of iron ions on GO sheets, the suspension was further stirred for 30 min. 0.94 M $NaBH_4$ was then added to the mixture dropwise at a 4.5 mL/min flow rate under vigorous stirring. After completion, the mixture was further stirred for 20 min to assure complete reduction (Khandelwal et al., 2021; Ren et al., 2018). The obtained black color precipitate was separated and washed repeatedly with water and ethanol before vacuum drying.

2.4. Characterization of composites

After synthesis, materials were characterized for (i) morphology and composition using high-resolution transmission electron microscopy (HRTEM) and EDS, (ii) surface area and pore size distribution using Brunauer Emmett-Teller (BET) method and density functional theory (DFT), respectively, (iii) zeta potential using electrophoretic mobility and DLS, (iv) crystallinity and phases using pXRD, (v) surface functionality using FTIR spectroscopy and (vi) surface composition using X-ray photoelectron spectroscopy (XPS). Detailed information about sample preparation and instrumentation is provided in the supplementary information.

2.5. Batch sorption experiments for initial efficiency evaluation

Solutions (20 mL 0.01 M $NaNO_3$) containing mono and multi-ionic metal species and different dyes (C_0 = 20 mg/L, pH = 6.5) were reacted for 12 h with 20 mg of adsorbent at 200 RPM and 25 °C. Three different experimental systems were as following- (i) solutions contaminated with mono-ionic metal species, i.e., CrO_4^{2-}, AsO_2^-, Ni^{2+} and Cd^{2+}, (ii) multi-metal contaminated solutions containing both metal cations and oxy-anions, and (iii) solutions containing organic dye of varying ionic nature, i.e., cationic methylene blue (MB), anionic methyl orange (MO) and zwitterionic rhodamine-B (RB) After the interaction, reaction mixtures were centrifuged, and solutions were analyzed for metals concentration using ICP-OES and dyes using UV–Vis spectrophotometer. Kinetic tests were performed by varying the interaction time (0–12 h), and data were fitted with non-linear pseudo-first, pseudo-second, and general order kinetic models (Moussout et al., 2018; Saucier et al., 2015). Similarly, contaminants concentration was varied (10–100 mg/L) by keeping adsorbent mass and interaction time constant to analyze maximum sorption capacities. Obtained data were fitted with non-linear Langmuir, Freundlich, and Sip isotherm models to get further insights into the nature of sorption (Ayawei et al., 2017). To assess the impact of pH on sorption, the initial solution pH was varied from 3 to 9. Further, river water, synthetic groundwater, and synthetic seawater (compositions given in Table S1 and Table S2) were spiked with 20 mg/L concentration of contaminants and reacted with composite to evaluate their efficiencies in complex natural matrices. After the interaction, reaction precipitates were collected and thoroughly characterized for change in morphology, crystallinity, and surface functionality to visualize involved removal mechanisms. XPS analysis was performed to confirm reductive sorption of toxic metal species. Details of various kinetic and isotherm models, XPS sample analysis, and physicochemical parameters of used aqueous matrices are provided in the supplementary information.

2.6. Continuous separation of contaminants: Column experiments

It is essential to understand adsorbents' sorption behavior and capacity in separating contaminants under continuous filtration mode to ascertain real environmental applications (De Gisi et al., 2016). A column of dimension 11.5 cm x 0.65 cm was sequentially filled with quartz sand (1.5 g), sand-composite mixture (900 mg sand + 100 mg composite), and quartz sand (1.5 g). A piece of sponge was added at both the ends of the tightly packed column. All three contaminant systems studied in batch mode were used to understand the reactive transport of metals and dyes in continuous columns containing the composite as a fixed adsorbent bed. The influent concentration of each contaminant was kept at 10 mg/L. At first, columns were utterly saturated with water then contaminated waters were passed against the gravity at a flow rate of 0.5 mL/min using a peristaltic pump. Columns containing quartz sand have served as blanks for the experiments. Effluents were collected in 15 mL tubes and analyzed for released metals and dyes concentrations. Obtained experimental data were further modeled using the Thomas column transport model to get details of continuous filtration rate and separation efficiency (Chowdhury et al., 2013). Model details are provided in the supplementary information.

2.7. Material regeneration and secondary contaminant leaching tests

The regeneration and reuse potential of the GOI composite for toxic metals and dyes was evaluated through multiple adsorption–desorption cycles. For metal regeneration, the spent composite was washed with a pH = 3 acidic solution, while methanol was used for dye desorption and material recovery. The regenerated composite was then reused in subsequent adsorption cycles to assess its removal efficiency. To investigate secondary contaminant leaching, spent adsorbents containing sorbed metals and dyes were exposed to simulated rainwater (pH = 4.5), and the desorbed fraction was analyzed. Additionally, the stability of the composite was assessed by monitoring the release of iron ions during performed batch and column experiments.

3. Results and discussion

3.1. Characterization of Fe^0 impregnated graphene

HRTEM images showed that bulk GO sheets (Fig. 1a) were delaminated to graphene and also fragmented after sonication and Fe^0 nanoparticles growth on the surface (Fig. 1b). These particles were very small and spherical in nature with a very thin or invisible layer of oxide shell. Observation was further supported with the TEM-EDS analysis and elemental mapping in Fig. S1 showing Fe/O ratio = 0.86 which is high compared to iron oxides (Zhu et al., 2017). Most of the particles were of diameter < 50 nm and were well dispersed on graphene surface in Fe^0 impregnated graphene (GOI) nanocomposite. After the interaction with contaminants a clear and thick oxide shell generated confirming the surface transformation (Zhu et al., 2017).

pXRD spectra (Fig. 1d) has shown that characteristic d 001 peak of GO at 11.6° disappeared after Fe^0 growth which suggest a drastic decrease in the interlayer spacing of GO (Mehrabi et al., 2019). Characteristic peak of Fe^0 at 44.8° was appeared in GOI composite while other peaks associated with crystalline iron oxide phases were absent, supporting the successful redox-state preservation of Fe^0 in GOI composite (Khandelwal et al., 2020). Graphene sheets generally act as potential electron storing agents which can capture released electrons from Fe^0 and later supply them back thereby helps in preserving and enhancing the reactivity of the composite (Zhang and Xi, 2011). FTIR spectra in Fig. 1e highlight GO associated peaks for C=C, C=O, C-OH and C-O stretching along with new peak at 590 cm^{-1} for Fe-O stretching in GOI nanocomposite (Huan et al., 2012). Further, zeta potential analysis at varying pH showed negative charged surface of GO with no point of zero charge. In contrast, after Fe^0 growth surface turned positive with a point of zero charge at pH = 7.4 (Fig. 1f). Whereas, without addition of acid and base the composite showed negative zeta potential at working pH of 6.5 in 0.01 M $NaNO_3$ background solution (Fig. 1g),

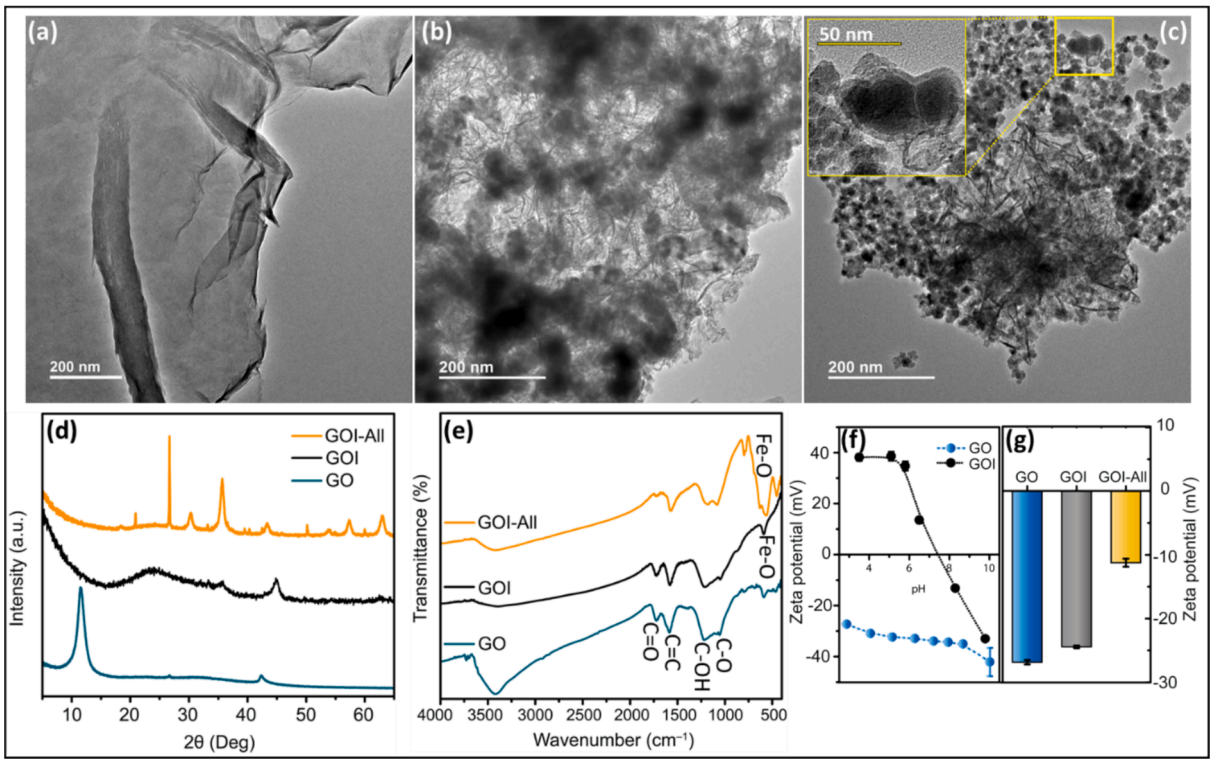

Fig. 1. HRTEM images of (a) GO, (b) GOI and (c) GOI after sorption of metals (inset- showing oxide shell over Fe^0), (d) pXRD, (e) FTIR, (f) zeta potential at varying pH in DI water and (g) zeta potential in 0.01 M $NaNO_3$ for adsorbents.

suggesting heterogeneous charge distribution on the surface and possibility of electrostatic attraction of both metal cations and oxi-anions. Further, zeta potential of < -20 mV justifies suspension stability and therefore high reactivity of the GOI composite (Paszkiewicz et al., 2016). BET-N_2 adsorption–desorption isotherm analysis (Fig. S2) showed a drastic increase in surface area (51.15 m^2/g) and pore volume (0.093 cc/g) after the delamination of bulk GO having surface area of 4.26 m^2/g and pore volume of 0.004 cc/g, and Fe^0 growth.

3.2. *Surface electron transfer and contaminants removal mechanisms*

After interaction with the contaminants GOI composite reaction precipitates were thoroughly characterized for change in surface morphology, elemental distribution, crystallinity, functionality, charge and redox distribution of surface species. HRTEM image in Fig. S3 show generation of a thick oxide shell on nZVI spheres after removal of toxic metals. In addition, elemental mapping and line scan data showed homogeneous presence of Cr, As, Ni and Cd on the surface of GOI composite suggesting their sorption on the surface. pXRD data after multi-contaminants removal showed absence of Fe^0 peak and generation of intense iron oxide peaks supporting electron transfer in the system (Fig. 1d). Similarly, FTIR peak associated with Fe-O stretching at 590 cm ^{1} disappeared after the multi-metals sorption and new Fe-O stretching at 570 cm ^{1} and 630 cm ^{1} generated corresponding to magnetite (Fe_3O_4) and γ-Fe_2O_3 (maghemite) respectively (Stoia et al., 2016). Further intense peak at 805 cm ^{1} which corresponds to bulk hydroxyl group bending in goethite (α-FeOOH) justifies iron oxidation and iron oxy-hydroxide generation (Liu et al., 2017). All the observations justified intense electron transfer on the surface of GOI composite. In addition to morphology, crystallinity and surface functionality, zeta potential of the composite has decreased to < -12 mV suggesting involvement of electrostatic attraction in the contaminant removal process. This decrease in zeta potential to below 20 mV also suggests the self-sedimentation probability of the particles after contaminants removal.

Since elemental iron nanoparticles have the redox potential of 0.44 V for Fe^{2+}/Fe^0, they can reduce the chromium which has a much higher redox potential of + 1.36 V for CrO_4^{2-}/Cr(III) couple. Arsenic used in the study had reduced form i.e. As(III). Whereas, redox potential of nickel (Ni^{2+}/Ni^0 = -0.24 V) and cadmium (Cd^{2+}/Cd^0 = -0.40 V) were comparable to iron and therefore could be removed through complexation and co-precipitation mechanism. (Khandelwal and Darbha, 2021) Further, to confirm the redox transformation of the contaminants, XPS was performed. Results in Fig. 2 a-h show the XPS survey scan and narrow range fittings for different contaminants. XPS survey scan in Fig. 2a shows the presence of C, Fe, and O on the surface of GOI composite. Zoom in image in Fig. 2b for Fe2p region showed presence of intense peaks in the range 700–740 eV due to different Fe-O structures suggesting the presence of iron oxides on the surface of GOI composite (Zhang et al., 2018). Further, presence of a peak at 706.9 eV corresponding to Fe^0 in GOI composite (Martindale and Reisner, 2016) (Fig. 2b) which disappeared after the sorption of contaminants suggesting oxidation of GOI and active surface electron transfer (Hu et al., 2019). Measurements and sample handling in aerobic atmosphere can lead to surface Fe-O species in XPS. However, observations from pXRD where no Fe-O associated crystalline mineral phase was observed and XPS where Fe-O peaks were present, suggest that the GOI composites were having a very thin amorphous iron-oxide shell on nZVI surface before interaction with contaminants.

Adsorbate specific removal mechanisms were further delineated through peak deconvolution in narrow range. Peak fitting in Cr2p region show (Fig. 2c) two different peaks at 577.1 eV and 579.8 eV corresponding to Cr(III) and Cr(VI), respectively (Biesinger et al., 2004). Surface characterization confirms dominant reduction of Cr(VI) to Cr (III) and also presence of some amount of Cr(VI) on GOI surface.

After interaction with chromium, FTIR spectra showed broadening of 590 cm ^{1} peak of GOI and 688 cm ^{1} peak corresponding to asymmetric Fe-O stretching appeared (Liu and Zhang, 2014). New band at 880 cm ^{1} was due to FeOOH (Fig. 3b). pXRD spectra (Fig. 3a) showed a decrease in Fe^0 peak and increase in the intensity of 35^0 Fe_2O_3 and 33^0 Fe_3O_4

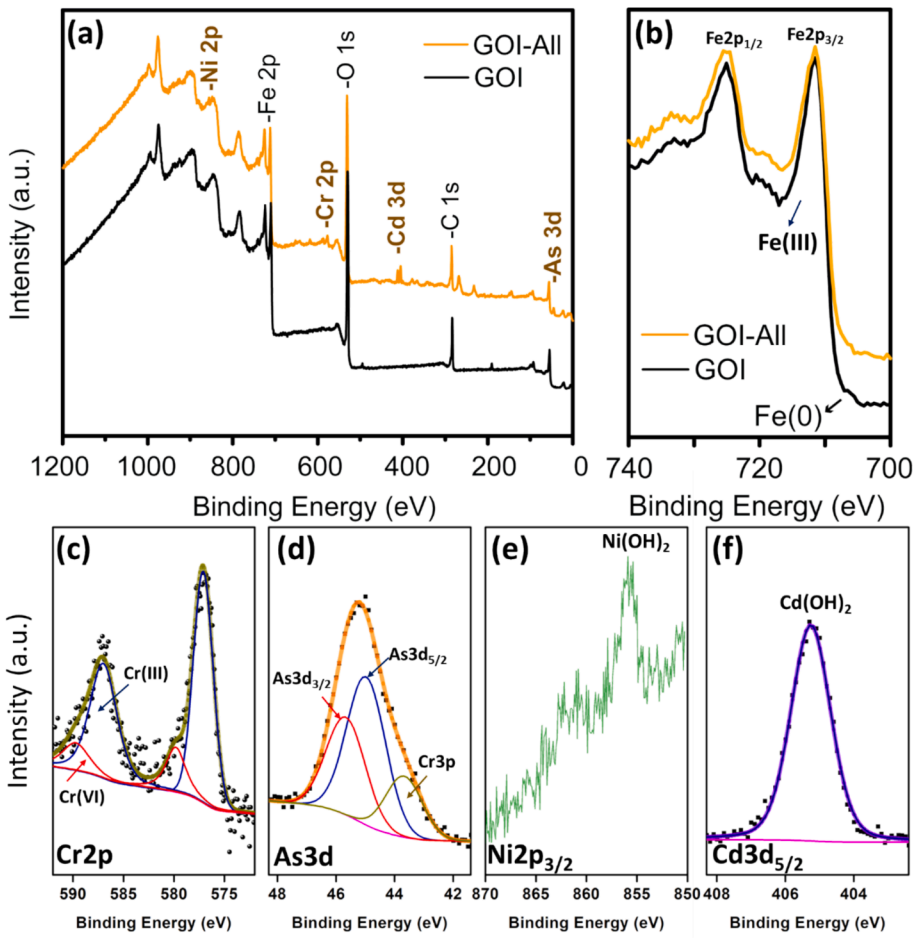

Fig. 2. (a) XPS survey scan for GOI composite before and after sorption of metals, and high-resolution spectra for (b) Fe2p (c) Cr2p, (d) As3d, (e) $Ni2p_{3/2}$ and (f) $Cd3d_{5/2}$ region.

peaks. Observations further confirmed partial oxidation of GOI surface and removal of chromium through both sorption and reductive co-precipitation.

Arsenic used in the study was in form of As(III), a reduced form. After the removal GOI composite showed $As3d_{5/2}$ peak at 45.0 eV binding energy assigned to As(III)-O (Fig. 2d). pXRD spectra showed presence of 27^0 strong FeOOH peak in addition to above stated iron oxide peaks. Similarly, FTIR spectra was observed to be very different than GOI with the presence of several –OH associated peaks at 880 cm ^{1}, 1010 cm ^{1} and 1632 cm ^{1} due to goethite (Lou et al., 2019; Liu et al., 2014) with less intense 690 cm ^{1} peak and a shifting in 570 cm ^{1} peak (Fig. 3b). Based on all these observations, arsenic removal can be attributed to its complexation with iron-oxy-hydroxides and co-precipitation on GOI surface. Whereas, even though intense oxidation of Fe^0 was observed in presence of Ni^{2+} and Cd^{2+}as confirmed by the absence of 44.6^0 Fe^0 peak, generation of intense iron oxide peaks in pXRD spectra (Fig. 3a), both nickel ($Ni2p_{3/2}$ at 855.9 eV binding energy) and cadmium ($Cd3d_{5/2}$ at 405.3 eV binding energy) have shown presence of $Ni(OH)_2$ and $Cd(OH)_2$ as dominant surface species on GOI as observed by XPS (Fig. 2e-f), suggesting no reduction (Zhu et al., 2017). This can also be supported with their comparative redox potential to iron. Similarly, FTIR spectra showed only 580 cm ^{1} and 630 cm ^{1} Fe-O stretching after nickel and cadmium removal (Fig. 3b). All these observations justify the removal of nickel and cadmium dominantly involved electrostatic attraction and coprecipitation with iron-oxyhydroxides on GOI surface. Since we only observed slight thickening of oxide shell of Fe^0 on GOI surface in presence of arsenic and chromium, it can be speculated that sorption/complexation and coverage of GOI surface with these adsorbates and thick iron oxyhydroxide layer (around 1.5 nm as shown in Fig. 1c inset) was resulting in blocking of further electron transfer from the Fe^0 core.

Zeta potential values for reaction precipitates (Fig. 3c) containing varying adsorbates were quite different which can further support the deduced removal mechanisms. For example, after chromium removal, zeta potential of GOI composite turned to positive (+7 mV) due to its reduction in Cr(III) and precipitation as $Cr(OH)_3$ with ferrihydrites. Whereas As(III)-O complexation with GOI surface resulted in increased negative zeta potential of 40 mV. In contrast, electrostatic attraction and coprecipitation of cationic metal species Cd^{2+} and Ni^{2+} resulted in positive zeta potential of GOI composite. (Khandelwal and Darbha, 2021).

Similarly, for dyes, in case of MB and RB, 44.8^0 Fe^0 peak intensity decreased (Fig. 3d) and iron-oxide associated peaks generated around 33^0 (magnetite), 35^0 (Fe_2O_3), 43^0 (maghemite) and 27^0 (FeOOH). MB reduction to leuco-methylene blue and its co-precipitation with iron-oxy-hydroxide as reported in earlier works (Khandelwal et al., 2021; Sun et al., 2015). At the same time, Fe^0 associated peak completely diminished in presence of MO with the generation of intense 30^0 and 35^0 iron-oxide peaks. Since Fe^0 can reduce the dye molecules, it breaks the chromophore by decomposing the –N=N- bond resulting in the decolorization of the solution of MO (Han et al., 2015). Therefore, we also obtained only 570 cm ^{1} and 630 cm ^{1} Fe-O stretching in the FTIR spectra of GOI composite after MO removal (Fig. 3e). Zeta potential of dye reaction precipitates have shown a decrease in negative potential after MB removal and increased negative zeta potential (Fig. 3f) after removal of MO and RB. This can be attributed to cationic nature of MB, and anionic nature of MO.

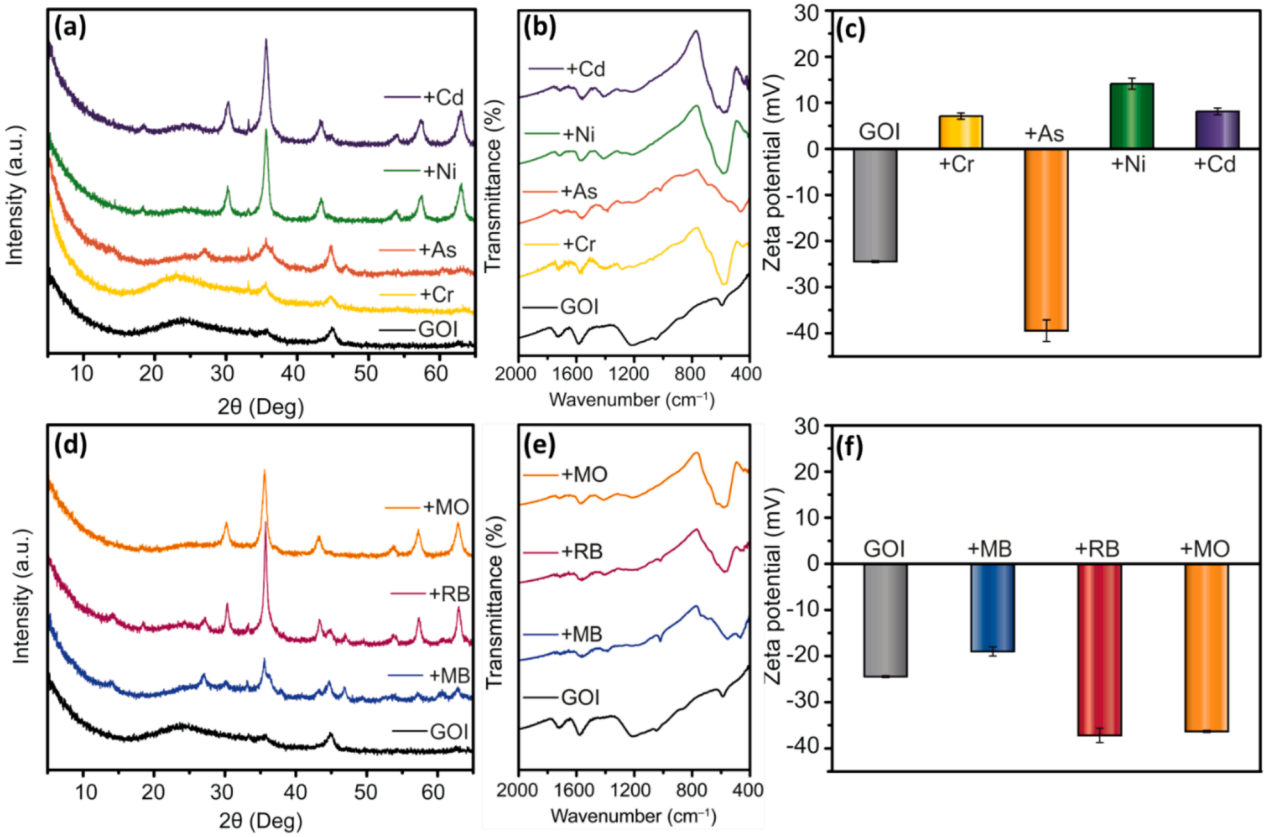

Fig. 3. (a, d) pXRD, (b, e) FTIR and (c, f) zeta potential of GOI composite before and after the sorption of metallic species and dyes, respectively.

3.3. Remediation of mono and multi-metallic contaminated solutions: Batch mode

Preliminary experiments for sorption of various metal cations and oxy-anions with GO and GOI composite showed their limited removal with GO (<10 mg/g) compared to GOI composite (>17 mg/g) suggesting presence of limited sorption sites on GO and its limited affinity for toxicants than synthesized GOI nanocomposite (Fig. 4a). Removal kinetics data in Fig. 4b confirmed very fast interaction of both cationic and anionic species with GOI composite. Sorption equilibrium for As and Cd was achieved within 5 min of interaction whereas it was 3 h for Ni and Cr. Out of fitted kinetic models (Table S4 and Fig. 4b), based on R^2 values, both pseudo second order model and general order model showed a good fit but non-linear least square errors (NLLS) i.e. RMSE and MRE values suggest better fit of general order model in most cases with the derived reaction order n > 7 justifying ultrafast interaction of contaminants with the composites (dos Reis et al., 2021). Obtained fitting parameters for different kinetic models are provided in Table S4. These results also justify the earlier interpretations obtained by thorough surface characterization of reaction precipitates in section 3.2.

Water bodies generally have contamination with multiple metal cations and oxi-anions, therefore, it is essential to test simultaneous removal of multiple species and total contaminant removal capacity of the composite (Gautam et al., 2015). To deduce the same, sorption isotherm experiments were performed in both mono and multi-metal contaminated solutions. Results in Fig. 5a and 5b show that Ni^{2+} and CrO_4^{2-} nearly achieved a plateau with increasing initial concentration. In contrast, As and Cd have shown continuous increase in sorption capacity

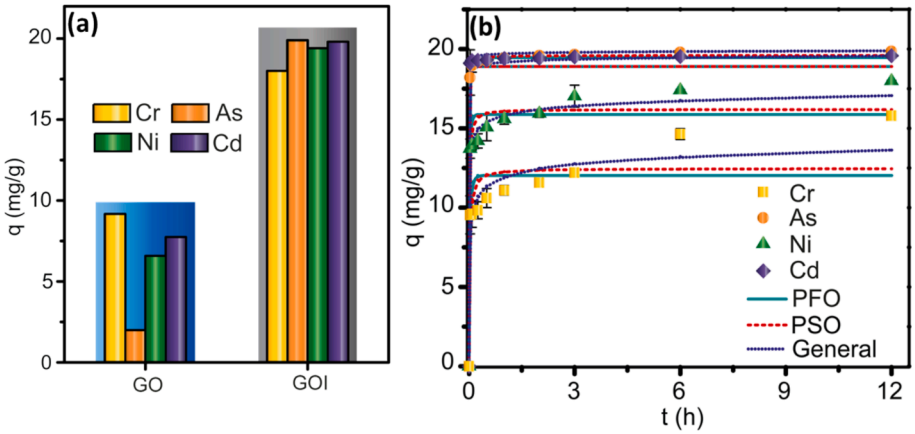

Fig. 4. (a) sorption capacity of GO and GOI composite in multi-metallic solutions, and (b) removal kinetics for GOI composite.

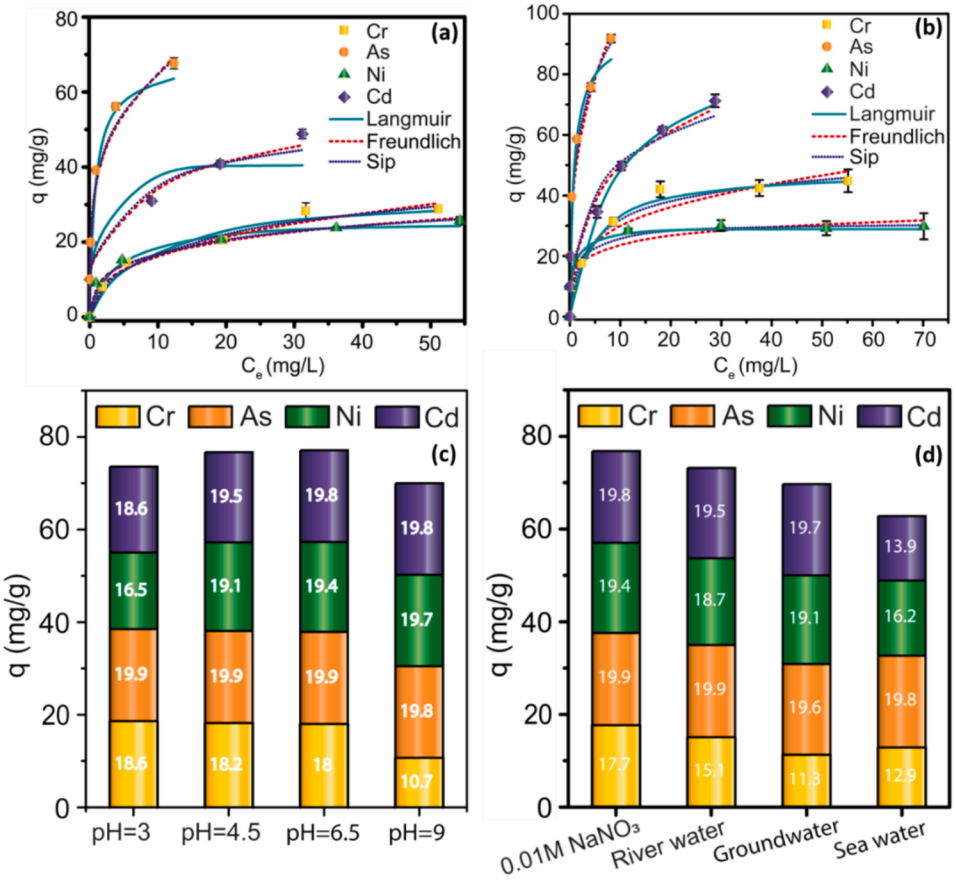

Fig. 5. Effect of initial contaminant concentration and sorption isotherm modelling in (a) mono and (b) multi-metallic solutions, effect of (c) solution pH and (d) complex water matrices on the total metal sorption capacity of GOI composite.

of composite with increasing contaminant concentration, suggesting heterogeneous sorption in both mono and multi-metallic solutions (Ayawei et al., 2017). In most of the cases, sorption isotherm data was well fitted with Sip isotherm model confirming heterogeneous nature of adsorbent surface (Tiwari et al., 2019). Removal capacity of the composite for all ionic species increased in multi-metallic system compared to mono-metallic system suggesting multi-layer stacking of different contaminants on GOI composite. Maximum sorption capacities (Tables S3 and S4) obtained from Sip model were Ni (30.5 mg/g) < Cr (49.8 mg/g) < Cd (93.7 mg/g) < As (143.6 mg/g) in mono-metallic system. The order of removal in multi-metallic system remained same with sorption capacities Ni (31.9 mg/g) < Cr (57.9 mg/g) < Cd (101.1 mg/g) < As (152.7 mg/g). Calculated non-linear least square (NLLS) errors are provided in Tables S3 and S4. In most of the cases, obtained error values were < 5 %.

Total metal removal capacity for GOI composite was found to be 343.6 mg/g emphasizing GOI as a potential sorbent for simultaneous removal of multiple contaminant species. Attributing to surface protonation and positive zeta potential in acidic pH, GOI composite has shown increased removal of CrO_4^{2-} and a slight decrease was observed for Cd^{2+} and Ni^{2+} (Fig. 5c) (Zhang et al., 2020). Removal of chromate ions decreased significantly at alkaline pH due to electrostatic repulsion. Removal of arsenic had no significant impact of solution pH due to its oxidation and strong complexation with iron-oxy-hydroxides (Sherman and Randall, 2003).

Circum-neutral pH was found to be optimum with highest total capacity to remove contaminants justifying environmental applicability of the composite. Finally, sorption of metal cations and oxy-anions was evaluated in different complex environmental matrices. Results in Fig. 5d show efficient removal of all ionic species from different waters. The order of total metal sorption capacities was 0.01 M $NaNO_3$ (76.8 mg/g) > river water (73.2 mg/g) > groundwater (69.6 mg/g) > sea water (62.9 mg/g). All ionic species followed the same order of removal capacities in these matrices. A slight decrease in the removal in these matrices can be attributed to presence of other major competitive ionic species in the system covering the sorption sites on GOI composite. Arsenic removal had no significant effect of water matrices with > 99 % removal in all waters due to its strong and selective complexation with iron-oxy-hydroxides.

3.4. *Batch sorption of organic dyes*

Graphene has the potential to sorb dye molecules and with addition of Fe^0 nanoparticles contributing to electron storage and release on the surface, GOI composite can reduce or degrade the dye molecules (Wang et al., 2015). Kinetic data in Fig. 6a showed instantaneous attraction and removal of dyes of different ionic behavior. Compared to cationic MB and anionic MO, a slight slower removal was observed for RB. Complete decolorization was observed for all dyes within 30 min of interaction with GOI composite. A good fit of data was observed with general order kinetic model and parameters are provided in Table S5. Further analysis of maximum sorption capacities using sorption isotherm modelling in Fig. 6b and Table S5 showed MB (81.3 mg/g) > MO (79.7 mg/g) > RB (31.7 mg/g). Efficient and faster removal of both cationic MB and anionic MO further supports heterogeneous nature of GOI surface.

GOI composite further showed efficient removal of all dyes in a wide pH range with optimum 100 % removal at circum-neutral pH (Fig. 6c). A slight decrease in removal at acidic pH for MB and at both acidic and alkaline pH for MO was observed. RB removal remained unaltered at all studied pH. Dye removal was 100 % in all complex water matrices

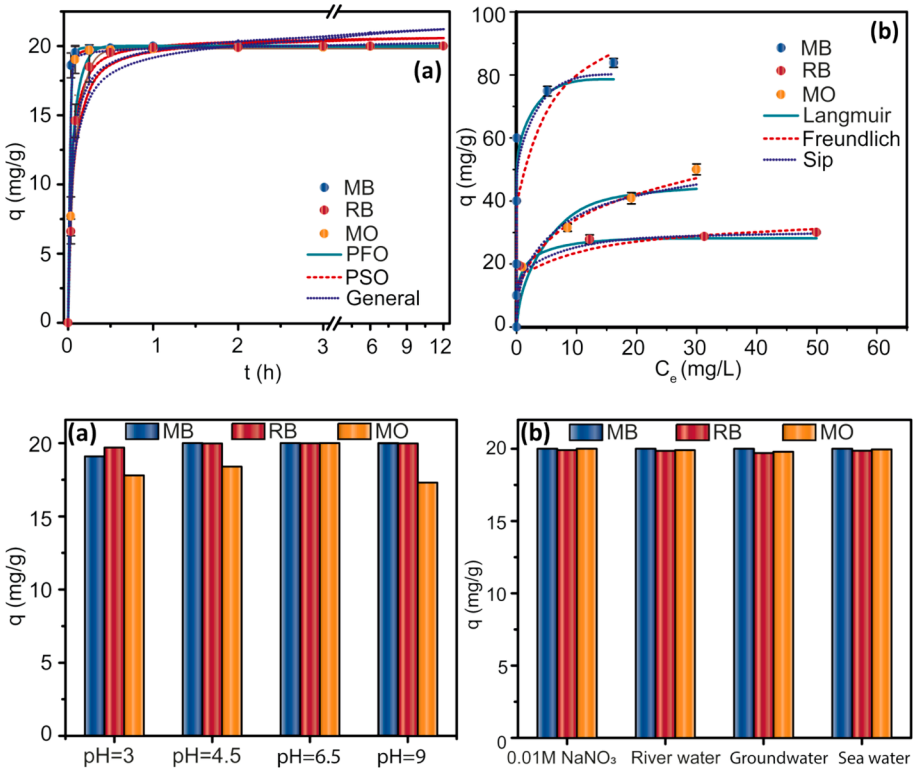

Fig. 6. Effect of (a) interaction time and (b) initial contaminant concentration with kinetic and sorption isotherm modelling, respectively (c) solution pH and (d) complex water matrices on dyes removal capacity of GOI composite.

(Fig. 6d). Complete decolorization of river, ground and sea water justifies the wide-scale applicability of the composite. Immediate and ultrafast interaction of dye molecules with the GOI composite and high dye sorption capacity suggested the potential of the material in continuous water decolorization.

3.5. *Reactive transport and continuous column retention of contaminants*

Present study, for the first time, delineates the column retention behavior of contaminants and in-turn continuous water filtration capacity of GOI nanocomposite. Results in section 3.4 showed wide scale applications of GOI composite in removing both inorganic and organic contaminants from complex water matrices. These batch sorption studies showed faster removal kinetics with high sorption capacities of GOI composite for contaminants justifying its potential in continuous water filtration. To test it, column transport experiments were performed (Tables S3–S6). Compared to blank sand column, composite containing columns have shown very high retention of metals and dyes (Fig. 7a-c).

In the studied pore volume range, release of contaminants was increased with time. As observed in batch mode experiments, in both mono and multi-metallic systems, Ni^{2+} released earlier compared to other ions. In presence of dyes, elution order was as following- MO, RB and MB. Experimental data obtained from column transport were fitted well with the Thomas model (Patel, 2019). Column retention efficiency in mono-metallic solutions (Table S3) was Ni (16.4 mg/g) < As (21.2 mg/g) < Cd (22.2 mg/g) < Cr (37.8 mg/g). While in multi-metal contaminated solutions retention efficiencies (Table S4) order changed to Ni (15.8 mg/g) < As (19.4 mg/g) < Cr (24.2 mg/g) < Cd (24.4 mg/g). In case of multi-metallic solutions, a slight decrease in individual metal retention capacity compare to mono-metallic solutions and column saturation ($C/C_0 > 0.8$) was observed which can be attributed to competitive sorption of metals, faster Fe-O layer thickening and consumption of active sites.

Total metal retention efficiency or breakthrough capacity was observed to be 84 mg/g suggesting very high continuous metal filtration capacity of GOI composite. Similarly, for dye contaminated waters, continuous retention efficiency order (Table S5) was MO (24.4 mg/g) < RB (32.2 mg/g) < MB (39.8 mg/g). Overall, a good retention of both metals and dyes justifies the continuous contaminant filtration capacity of the GOI composite and its candidature in water and wastewater treatment applications.

3.6. *Regeneration and reuse possibilities and secondary contaminant leaching*

Material stability, secondary contamination due to release of sorbed pollutants and constituent ions and regeneration or reuse possibility are the key factors to be considered while exploring field-scale applications. Therefore, regeneration and reuse of composite was explored for toxic metals and dyes. Washing with a pH = 3 solution was done for regeneration in case of metals while methanol was used to recover dyes and regenerate material.

Results showed that composite maintained removal capacity above 80 % in three studied cycles in case of chromium and arsenic while capacity decreased nearly up to 50 % in case of cadmium and nickel. In all three cycles, release of metals in wash at acidic pH was observed to be comparatively less than the sorbed amount (Fig. S4). For instance, arsenic showed < 10 % release in both mono and multi-contaminant solutions confirming strong chemisorption of contaminants on composite surface.

In case of dyes (Fig. S5), material showed > 80 % removal in all three cycles suggesting high reusability. Also, methylene blue showed < 10 % recovery in all methanol wash cycles whereas recovery % increased to nearly 50 % and 70 % in third cycle for MO and RB, respectively. This suggests possible degradation of MB and initially supplied RB and MO followed by strong adsorption and desorption of RB and MO on the surface in later cycles by generated iron oxy-hydroxides and graphene.

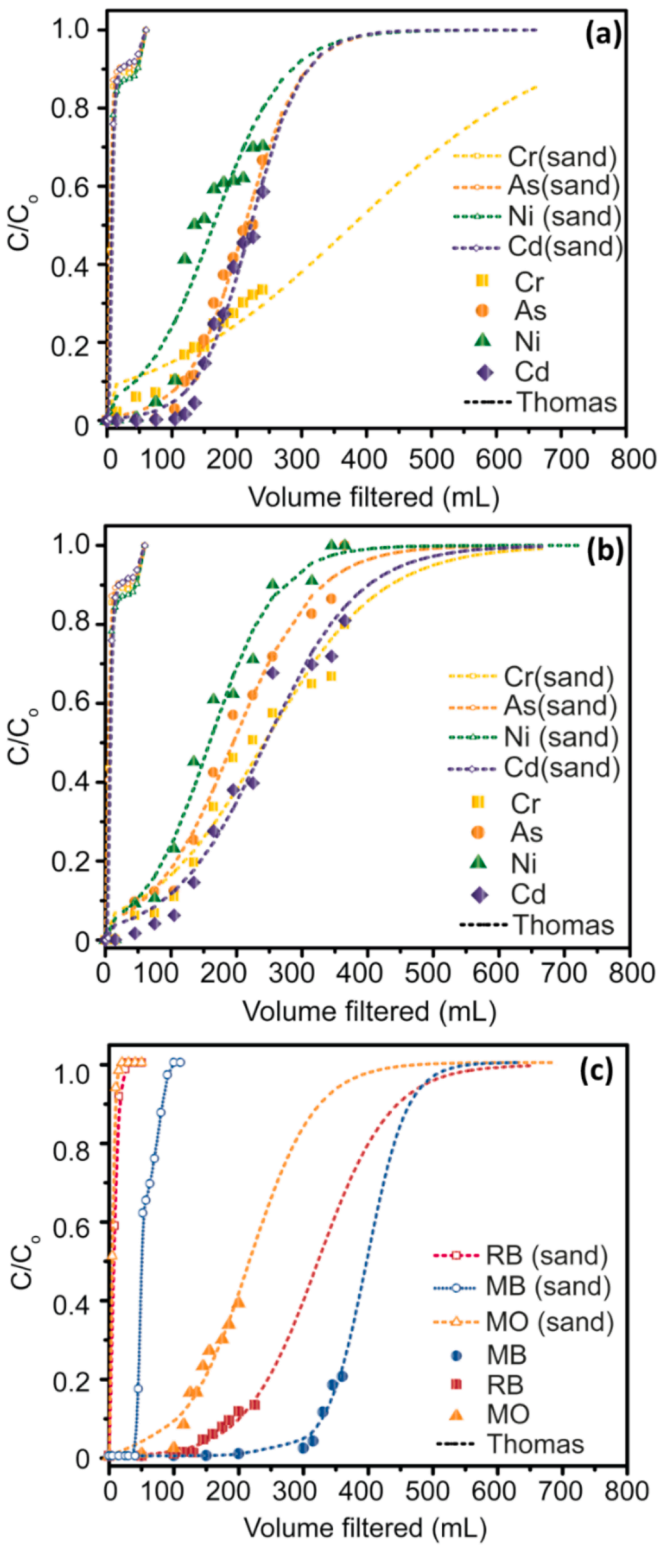

Fig. 7. Reactive transport and continuous column breakthrough curves for (a) mono and (b) multi-metal contaminant system and (c) dyes in presence of GOI composite.

Secondary release of sorbed dyes and toxic metals in the environment from spent nano-adsorbents can pose serious disposal concern and to explore the same, contaminant containing spent materials were interacted with rain water (Fig. S6a). Except arsenic which showed 6.6 % and 1.5 % desorption in mono and multi-metallic spent adsorbents, all other metals showed < 0.5 % desorption in rain water, suggesting strong binding with minimal possibility of secondary contamination. In case of dyes, desorption was observed to be < 10 % (Fig. S6b). Release of constituent ions from the sorbent can pose another challenge of material stability. Therefore, release of iron ions was monitored during all the performed batch and column experiments. In all the cases of performed batch and column filtration tests (Fig. S7) except pH = 3, dissolution was found well below 2 mg/L (prescribed safe limit). Even at pH = 3, the release was observed to be only around 6.9 mg/L (Fig. S8), corresponding to 0.69 % of the total catalyst used. This suggests minimal loss of the composite at acidic pH. It can be attributed to metals reduction with simultaneous oxidation of iron to insoluble iron-oxy hydroxides. Results confirm high material stability, reusability and strong binding capacity of the material along with minimal secondary desorption and leaching in rain water.

4. Conclusions: Environmental applications perspective

The study concludes GOI composite as a potential adsorbent for the removal of both organic and inorganic contaminants from varying environmental matrices. GOI composite can also handle multi-metal contamination with the efficiency reaching to > 340 mg/g. Synthesis of bulk graphene is cheaper and easy in comparison to single layer graphene therefore simultaneous bulk-graphene delamination and iron growth can be an affordable option in terms of scalability. GO surface helped in good dispersion of Fe^0 particles and also preserves their redox state in GOI composite which also showed very high electron transfer potential. GOI can participate in the removal of contaminants through various mechanisms ranging from reductive sorption of chromium to complexation of arsenic and co-precipitation with formed iron-oxyhydroxides. Fenton oxidation in the system may occur and result in degradation of organic contaminants including dyes. In presence of GOI composite, continuous column retention of both metals and dyes was higher than blank sand columns. In multi-metal contaminated solutions, total continuous filtration capacity was 84 mg/g. This suggests that the material is capable in continuously filtering 84,000 L of water containing 1 mg/L of total metals concentration with 1 kg of the composite. Cost analysis (Table S6) suggests that the water purification cost will be approximately 2800 L/USD.

The GOI composite demonstrated high stability and reusability, maintaining over 80 % removal efficiency in multiple regeneration cycles for chromium, arsenic, and dyes. Minimal secondary desorption of metals and dyes in rainwater suggests strong contaminant binding, reducing the risk of secondary pollution. These findings highlight the potential of GOI composite for long-term practical applications in water treatment. Research efforts should be made in developing green methods for the bulk scale synthesis of GO followed by one-step synthesis of GOI composite. Therefore, current study confirms the potential of GOI composite in continuous water filtration at laboratory scale which should be further investigated and optimized at field scale reactor setups for real environmental applications.

CRediT authorship contribution statement

Jai Kishan Rajak: Writing – original draft, Formal analysis, Data curation. **Nitin Khandelwal:** Writing – review & editing, Project administration, Investigation, Funding acquisition, Conceptualization. **Zahid Ahmad Ganie:** Writing – review & editing, Data curation. **Dieter Schild:** Writing – review & editing, Formal analysis. **Gopala Krishna Darbha:** Writing – review & editing, Supervision, Resources, Project administration, Funding acquisition, Conceptualization.

Declaration of competing interest

The authors declare that they have no known competing financial interests or personal relationships that could have appeared to influence the work reported in this paper.

Acknowledgments

NK would like to acknowledge the faculty initiation grant (FIG-10107) of IIT Roorkee; GKD appreciates the Core Research Grant from the Anusandhan National Research Foundation (ANRF), India (CRG/2021/006020) and the DBT project grant (BT/PR45809/BCE/8/1791/2023). ZAG expresses his gratitude for the SRF funding from UGC, India. Authors are further thankful to IISER Kolkata's central instrumentation facility for sample analysis (ICP-OES, FESEM, HRTEM, and pXRD).

Data availability

Data will be made available on request.

References

Das, R., Vecitis, C.D., Schulze, A., Cao, B., Ismail, A.F., Lu, X.B., Chen, J.P., Ramakrishna, S., 2017. Recent advances in nanomaterials for water protection and monitoring. Chem Soc Rev 46 (22), 6946–7020. https://doi.org/10.1039/c6cs00921b.

Perreault, F., de Faria, A.F., Elimelech, M., 2015. Environmental applications of graphene-based nanomaterials. Chem Soc Rev 44 (16), 5861–5896. https://doi.org/10.1039/c5cs00021a.

Sur, U.K., 2012. Graphene: A Rising Star on the Horizon of Materials Science. International Journal of Electrochemistry 2012, 237689. https://doi.org/10.1155/2012/237689.

Dideikin, A.T., Vul, A.Y., 2019. Graphene Oxide and Derivatives: The Place in Graphene Family. Frontiers in Physics 6.

Shen, Y., Fang, Q., Chen, B., 2015. Environmental Applications of Three-Dimensional Graphene-Based Macrostructures: Adsorption. Transformation, and Detection, Environ Sci Technol 49 (1), 67–84. https://doi.org/10.1021/es504421y.

Plastiras, O.E., Deliyanni, E., Samanidou, V., 2021. Applications of Graphene-Based Nanomaterials in Environmental Analysis. Appl Sci-Basel 11 (7). https://doi.org/10.3390/app11073028.

Nadres, E.T., Fan, J.J., Rodrigues, D.F., 2016. Toxicity and Environmental Applications of Graphene-Based Nanomaterials. Carbon Nanostruct 323–356. https://doi.org/10.1007/978-3-319-45639-3_11.

Fanourakis, S.K., Peña-Bahamonde, J., Bandara, P.C., Rodrigues, D.F., 2020. Nano-based adsorbent and photocatalyst use for pharmaceutical contaminant removal during indirect potable water reuse. Npj Clean Water 3 (1), 1. https://doi.org/10.1038/s41545-019-0048-8.

Badhulika, S., Terse-Thakoor, T., Villarreal, C., Mulchandani, A., 2015. Graphene hybrids: synthesis strategies and applications in sensors and sensitized solar cells. Front Chem 3, 38. https://doi.org/10.3389/fchem.2015.00038.

Kruk, T., Warszyński, P., 2021. Conductive Nanofilms with Oppositely Charged Reduced Graphene Oxides as a Base for Electroactive Coatings and Sensors. Colloid Interfac 5 (2). https://doi.org/10.3390/colloids5020020.

Gupta, T., Ratandeep, M., Dutt, B., Kaur, S., Punia, S., Sharma, P.K.S.h., Pooja, L.S., 2024. Graphene-based nanomaterials as potential candidates for environmental mitigation of pesticides. Talanta 272, 125748. https://doi.org/10.1016/j.talanta.2024.125748.

Raman, C.D., Kanmani, S., 2016. Textile dye degradation using nano zero valent iron: A review. J Environ Manage 177, 341–355. https://doi.org/10.1016/j.jenvman.2016.04.034.

Khandelwal, N., Tiwari, E., Singh, N., Marsac, R., Schäfer, T., Monikh, F.A., Darbha, G.K., 2021. Impact of long-term storage of various redox-sensitive supported nanocomposites on their application in removal of dyes from wastewater: Mechanisms delineation through spectroscopic investigations. J Hazard Mater 401, 123375. https://doi.org/10.1016/j.jhazmat.2020.123375.

Khandelwal, N., Singh, N., Tiwari, E., Marsac, R., Schild, D., Schäfer, T., Darbha, G.K., 2023. Varying growth behavior of redox-sensitive nanoparticles on 1:1 and 2:1 clay surfaces: Mechanistic insights on preferential toxic ions removal in mono, co, and multi-metal contaminated waters. Chem Eng J 461. https://doi.org/10.1016/j.cej.2023.141883.

Guan, X., Sun, Y., Qin, H., Li, J., Lo, I.M., He, D., Dong, H., 2015. The limitations of applying zero-valent iron technology in contaminants sequestration and the corresponding countermeasures: the development in zero-valent iron technology in the last two decades (1994-2014). Water Res 75, 224–248. https://doi.org/10.1016/j.watres.2015.02.034.

Xing, R., He, J.J., Hao, P.L., Zhou, W.J., 2020. Graphene oxide-supported nanoscale zero-valent iron composites for the removal of atrazine from aqueous solution. Colloid Surface A 589. https://doi.org/10.1016/j.colsurfa.2020.124466.

Aher, A., Thompson, S., Nickerson, T., Ormsbee, L., Bhattacharyya, D., 2019. Reduced graphene oxide–metal nanoparticle composite membranes for environmental separation and chloro-organic remediation. Rsc Adv 9 (66), 38547–38557. https://doi.org/10.1039/C9RA08178J.

Wang, W., Cheng, Y.L., Kong, T., Cheng, G.S., 2015. Iron nanoparticles decoration onto three-dimensional graphene for rapid and efficient degradation of azo dye. J Hazard Mater 299, 50–58. https://doi.org/10.1016/j.jhazmat.2015.06.010.

Ren, J.W., Woo, Y.C., Yao, M., Lim, S., Tijing, L.D., Shon, H.K., 2019. Nanoscale zero-valent iron (nZVI) immobilization onto graphene oxide (GO)-incorporated electrospun polyvinylidene fluoride (PVDF) nanofiber membrane for groundwater remediation via gravity-driven membrane filtration. Sci Total Environ 688, 787–796. https://doi.org/10.1016/j.scitotenv.2019.05.393.

Fan, M.Y., Hu, J.W., Cao, R.S., Xiong, K.N., Wei, X.H., 2017. Modeling and prediction of copper removal from aqueous solutions by nZVI/rGO magnetic nanocomposites using ANN-GA and ANN-PSO. Sci Rep-Uk 7. https://doi.org/10.1038/S41598-017-18223-Y.

Masud, A., Soria, N.G.C., Aga, D.S., Aich, N., 2020. Adsorption and advanced oxidation of diverse pharmaceuticals and personal care products (PPCPs) from water using highly efficient rGO-nZVI nanohybrids. Environ Sci-Wat Res 6 (8), 2223–2238. https://doi.org/10.1039/d0ew00140f.

Zhu, H.J., Gao, H.Y., Huang, X.M., Kong, W.F., Yan, X.M., 2015. The uptake of europium by reduced graphene oxide-supported nanoscale zerovalent iron investigated by batch and modeling techniques. J Environ Chem Eng 3 (4), 2974–2980. https://doi.org/10.1016/j.jece.2015.10.014.

Li, Z.J., Wang, L., Yuan, L.Y., Xiao, C.L., Mei, L., Zheng, L.R., Zhang, J., Yang, J.H., Zhao, Y.L., Zhu, Z.T., Chai, Z.F., Shi, W.Q., 2015. Efficient removal of uranium from aqueous solution by zero-valent iron nanoparticle and its graphene composite. J Hazard Mater 290, 26–33. https://doi.org/10.1016/j.jhazmat.2015.02.028.

Zhang, F.J., Xuan, H., Xie, F.Z., Jiang, T., Chen, T., Oh, W.C., 2012. Enhancing Decolorization for Methyl Orange in Aqueous Solution by Graphene Supported Nanoscale Zero Valent Iron. Asian J Chem 24 (9), 3994–3996.

Yang, B., Tian, Z., Zhang, L., Guo, Y.P., Yan, S.Q., 2015. Enhanced heterogeneous Fenton degradation of Methylene Blue by nanoscale zero valent iron (nZVI) assembled on magnetic Fe3O4/reduced graphene oxide. J Water Process Eng 5, 101–111. https://doi.org/10.1016/j.jwpe.2015.01.006.

Xu, H., Tian, W.G., Zhang, Y.J., Tang, J., Zhao, Z.T., Chen, Y., 2018. Reduced Graphene Oxide/Attapulgite-Supported Nanoscale Zero-Valent Iron Removal of Acid Red 18 from Aqueous Solution. Water Air Soil Poll 229 (12). https://doi.org/10.1007/S11270-018-4033-5.

Mehrabi, N., Masud, A., Afolabi, M., Hwang, J., Ortiz, G.A.C., Aich, N., 2019. Magnetic graphene oxide-nano zero valent iron (GO-nZVI) nanohybrids synthesized using biocompatible cross-linkers for methylene blue removal. Rsc Adv 9 (2), 963–973. https://doi.org/10.1039/c8ra08386j.

Kumarathilaka, P., Jayaweera, V., Wijesekara, H., Kottegoda, I.R.M., Rosa, S.R.D., Vithanage, M., 2016. Insights into Starch Coated Nanozero Valent Iron-Graphene Composite for Cr(VI) Removal from Aqueous Medium. J Nanomater 2016. https://doi.org/10.1155/2016/2813289.

Li, J., Chen, C.L., Zhu, K.R., Wang, X.K., 2016. Nanoscale zero-valent iron particles modified on reduced graphene oxides using a plasma technique for Cd(II) removal. J Taiwan Inst Chem E 59, 389–394. https://doi.org/10.1016/j.jtice.2015.09.010.

Cao, R.S., Fan, M.Y., Hu, J.W., Ruan, W.Q., Wu, X.L., Wei, X.H., 2018. Artificial Intelligence Based Optimization for the Se(IV) Removal from Aqueous Solution by Reduced Graphene Oxide-Supported Nanoscale Zero-Valent Iron Composites. Materials 11 (3). https://doi.org/10.3390/Ma11030428.

Das, T.K., Sakthivel, T.S., Jeyaranjan, A., Seal, S., Bezbaruah, A.N., 2020. Ultra-high arsenic adsorption by graphene oxide iron nanohybrid: Removal mechanisms and potential applications. Chemosphere 253. https://doi.org/10.1016/j.chemosphere.2020.126702.

Yao, Y.H., Huang, S.M., Zhou, W., Liu, A.R., Zhao, W.J., Song, C.Y., Liu, J., Zhang, W.X., 2019. Highly dispersed core-shell iron nanoparticles decorating onto graphene nanosheets for superior Zn(II) wastewater treatment. Environ Sci Pollut R 26 (1), 806–815. https://doi.org/10.1007/s11356-018-3631-5.

Pan, Y., Cai, Y., Chen, L., Sun, L., Deng, L., Huang, R., 2024. Synthesis of a graphene oxide-based zerovalent iron nanocomposite for efficient remediation of Re(VII) from simulated wastewater in high pH. J Water Process Eng 65, 105767. https://doi.org/10.1016/j.jwpe.2024.105767.

Liu, X., Liu, W., Chi, Z., 2022. Reduced graphene oxide supported nanoscale zero-valent iron (nZVI/rGO) for in-situ remediation of Cr(VI)/nitrate-polluted aquifer. J Water Process Eng 49, 103188. https://doi.org/10.1016/j.jwpe.2022.103188.

Jha, A.K., Chakraborty, S., Biswas, J.K., 2024. Green synthesis of low-cost graphene oxide-nano zerovalent iron composite from solid waste for photocatalytic removal of antibiotics. iScience 27 (12). https://doi.org/10.1016/j.isci.2024.111486.

Shukla, P., Mahata, S., Sahu, A., Singh, M., Rai, V.K., Rai, A., 2017. First graphene oxide promoted metal-free nitrene insertion into olefins in water: towards facile synthesis of activated aziridines. Rsc Adv 7 (77), 48723–48729. https://doi.org/10.1039/C7RA09351A.

Khandelwal, N., Behera, M.P., Rajak, J.K., Darbha, G.K., 2020. Biochar-nZVI nanocomposite: optimization of grain size and Fe0 loading, application and removal mechanism of anionic metal species from soft water, hard water and groundwater. Clean Technol Envir 22 (5), 1015–1024. https://doi.org/10.1007/s10098-020-01846-7.

Ren, L.M., Dong, J., Chi, Z.F., Huang, H.Z., 2018. Reduced graphene oxide-nano zero value iron (rGO-nZVI) micro-electrolysis accelerating Cr(VI) removal in aquifer. J Environ Sci-China 73, 96–106. https://doi.org/10.1016/j.jes.2018.01.018.

Moussout, H., Ahlafi, H., Aazza, M., Maghat, H., 2018. Critical of linear and nonlinear equations of pseudo-first order and pseudo-second order kinetic models. Karbala International Journal of Modern Science 4 (2), 244–254. https://doi.org/10.1016/j.kijoms.2018.04.001.

Saucier, C., Adebayo, M.A., Lima, E.C., Cataluña, R., Thue, P.S., Prola, L.D.T., Puchana-Rosero, M.J., Machado, F.M., Pavan, F.A., Dotto, G.L., 2015. Microwave-assisted

activated carbon from cocoa shell as adsorbent for removal of sodium diclofenac and nimesulide from aqueous effluents. J Hazard Mater 289, 18–27. https://doi.org/10.1016/j.jhazmat.2015.02.026.

Ayawei, N., Ebelegi, A.N., Wankasi, D., 2017. Modelling and Interpretation of Adsorption Isotherms. J Chem-Ny 2017, 3039817. https://doi.org/10.1155/2017/3039817.

De Gisi, S., Lofrano, G., Grassi, M., Notarnicola, M., 2016. Characteristics and adsorption capacities of low-cost sorbents for wastewater treatment: A review. Sustain Mater Techno 9, 10–40. https://doi.org/10.1016/j.susmat.2016.06.002.

Chowdhury, Z.Z., Zain, S.M., Rashid, A.K., Rafique, R.F., Khalid, K., 2013. Breakthrough Curve Analysis for Column Dynamics Sorption of Mn(II) Ions from Wastewater by Using Mangostana garcinia Peel-Based Granular-Activated Carbon. J Chem-Ny 2013, 959761. https://doi.org/10.1155/2013/959761.

Zhu, S., Ho, S.-H., Huang, X., Wang, D., Yang, F., Wang, L., Wang, C., Cao, X., Ma, F., 2017. Magnetic Nanoscale Zerovalent Iron Assisted Biochar: Interfacial Chemical Behaviors and Heavy Metals Remediation Performance. Acs Sustain Chem Eng 5 (11), 9673–9682. https://doi.org/10.1021/acssuschemeng.7b00542.

Mehrabi, N., Masud, A., Afolabi, M., Hwang, J., Calderon Ortiz, G.A., Aich, N., 2019. Magnetic graphene oxide-nano zero valent iron (GO–nZVI) nanohybrids synthesized using biocompatible cross-linkers for methylene blue removal. Rsc Adv 9 (2), 963–973. https://doi.org/10.1039/C8RA08386J.

Khandelwal, N., Behera, M.P., Rajak, J.K., Darbha, G.K., 2020. Biochar-nZVI nanocomposite: optimization of grain size and Fe(0)loading, application and removal mechanism of anionic metal species from soft water, hard water and groundwater. Clean Technol Envir 22 (5), 1015–1024. https://doi.org/10.1007/s10098-020-01846-7.

Zhang, X.-F., Xi, Q., 2011. A graphene sheet as an efficient electron acceptor and conductor for photoinduced charge separation. Carbon 49 (12), 3842–3850. https://doi.org/10.1016/j.carbon.2011.05.019.

Huan, T.N., Van Khai, T., Kang, Y., Shim, K.B., Chung, H., 2012. Enhancement of quaternary nitrogen doping of graphene oxide via chemical reduction prior to thermal annealing and an investigation of its electrochemical properties. J Mater Chem 22 (29), 14756–14762. https://doi.org/10.1039/C2JM31158E.

Paszkiewicz, M., Gołąbiewska, A., Rajski, Ł., Kowal, E., Sajdak, A., Zaleska-Medynska, A., 2016. Synthesis and Characterization of Monometallic (Ag, Cu) and Bimetallic Ag-Cu Particles for Antibacterial and Antifungal Applications. J Nanomater 2016, 2187940. https://doi.org/10.1155/2016/2187940.

Stoia, M., Istratie, R., Păcurariu, C., 2016. Investigation of magnetite nanoparticles stability in air by thermal analysis and FTIR spectroscopy. J Therm Anal Calorim 125 (3), 1185–1198. https://doi.org/10.1007/s10973-016-5393-y.

Liu, A., Liu, J., Han, J., Zhang, W.-X., 2017. Evolution of nanoscale zero-valent iron (nZVI) in water: Microscopic and spectroscopic evidence on the formation of nano- and micro-structured iron oxides. J Hazard Mater 322, 129–135. https://doi.org/10.1016/j.jhazmat.2015.12.070.

Khandelwal, N., Darbha, G.K., 2021. Combined antioxidant capped and surface supported redox-sensitive nanoparticles for continuous elimination of multi-metallic species. Chem Commun 57 (59), 7280–7283. https://doi.org/10.1039/D1CC02972J.

Zhang, D., Li, Y., Tong, S., Jiang, X., Wang, L., Sun, X., Li, J., Liu, X., Shen, J., 2018. Biochar supported sulfide-modified nanoscale zero-valent iron for the reduction of nitrobenzene. Rsc Adv 8 (39), 22161–22168. https://doi.org/10.1039/C8RA04314K.

Martindale, B.C.M., Reisner, E., 2016. Bi-Functional Iron-Only Electrodes for Efficient Water Splitting with Enhanced Stability through In Situ Electrochemical Regeneration. Adv Energy Mater 6 (6), 1502095. https://doi.org/10.1002/aenm.201502095.

Hu, X., Tian, X., Lin, Y.-W., Wang, Z., 2019. Nickel foam and stainless steel mesh as electrocatalysts for hydrogen evolution reaction, oxygen evolution reaction and overall water splitting in alkaline media. Rsc Adv 9 (54), 31563–31571. https://doi.org/10.1039/C9RA07258F.

Biesinger, M.C., Brown, C., Mycroft, J.R., Davidson, R.D., McIntyre, N.S., 2004. X-ray photoelectron spectroscopy studies of chromium compounds. Surf Interface Anal 36 (12), 1550–1563. https://doi.org/10.1002/sia.1983.

Liu, A., Zhang, W.-X., 2014. Fine structural features of nanoscale zero-valent iron characterized by spherical aberration corrected scanning transmission electron microscopy (Cs-STEM). Analyst 139 (18), 4512–4518. https://doi.org/10.1039/C4AN00679H.

Lou, Y., Cai, Y., Tong, Y., Hsieh, L., Li, X., Xu, W., Shi, K., Shen, C., Xu, X., Lou, L., 2019. Interaction between pollutants during the removal of polychlorinated biphenyl-heavy metal combined pollution by modified nanoscale zero-valent iron. Sci Total Environ 673, 120–127. https://doi.org/10.1016/j.scitotenv.2019.04.064.

Liu, A.-R., Liu, J., Pan, B., Zhang, W.-X., 2014. Formation of Lepidococite (γ-FeOOH) from Oxidation of Nanoscale Zero-Valent Iron (nZVI) in the Oxygenated Water. RSC Adv. 4. https://doi.org/10.1039/C4RA08988J.

Sun, X., Kurokawa, T., Suzuki, M., Takagi, M., Kawase, Y., 2015. Removal of cationic dye methylene blue by zero-valent iron: Effects of pH and dissolved oxygen on removal mechanisms. Journal of Environ. Sci. Health, Part A 50 (10), 1057–1071. https://doi.org/10.1080/10934529.2015.1038181.

Han, L., Xue, S., Zhao, S., Yan, J., Qian, L., Chen, M., 2015. Biochar Supported Nanoscale Iron Particles for the Efficient Removal of Methyl Orange Dye in Aqueous Solutions. Plos One 10 (7), e0132067. https://doi.org/10.1371/journal.pone.0132067.

dos Reis, G.S., Larsson, S.H., Thyrel, M., Pham, T.N., Claudio Lima, E., de Oliveira, H.P., Dotto, G.L., 2021. Preparation and Application of Efficient Biobased Carbon Adsorbents Prepared from Spruce Bark Residues for Efficient Removal of Reactive Dyes and Colors from Synthetic Effluents. Coatings 11 (7). https://doi.org/10.3390/coatings11070772.

Gautam, R.K., Sharma, S.K., Mahiya, S., Chattopadhyaya, M.C., 2015. Chapter, 1 Contamination of Heavy Metals in Aquatic Media: Transport, Toxicity and Technologies for Remediation, Heavy Metals In Water: Presence, Removal and Safety, The Royal Society of. Chemistry 1–24. https://doi.org/10.1039/9781782620174-00001.

Tiwari, D., Bhunia, H., Bajpai, P., 2019. Synthesis, characterization, adsorption and thermodynamic studies of pure and binary CO2-N2 mixtures on oxygen enriched nanostructured carbon adsorbents. Braz J Chem Eng 36, 1319–1331. https://doi.org/10.1590/0104-6632.20190363s20180036.

Zhang, J., Lin, S., Han, M., Su, Q., Xia, L., Hui, Z., 2020. Adsorption Properties of Magnetic Magnetite Nanoparticle for Coexistent Cr(VI) and Cu(II) in Mixed Solution. Water-Sui 12 (2). https://doi.org/10.3390/w12020446.

Sherman, D.M., Randall, S.R., 2003. Surface complexation of arsenic(V) to iron(III) (hydr)oxides: structural mechanism from ab initio molecular geometries and EXAFS spectroscopy. Geochim Cosmochim Ac 67 (22), 4223–4230. https://doi.org/10.1016/S0016-7037(03)00237-0.

Patel, H., 2019. Fixed-bed column adsorption study: a comprehensive review. Appl. Water Sci. 9 (3), 45. https://doi.org/10.1007/s13201-019-0927-7.